Available online at www.sciencedirect.com
ScienceDirect
Journal of Catalysis 253 (2008) 28–36
JOURNAL OF CATALYSIS
www.elsevier.com/locate/jcat

Processing of hydrocarbons in an AC discharge nonthermal plasma reactor: An approach to generate reducing agents for on-board automotive exhaust gas cleaning

Yu Xing [a], Zhenxin Liu [b], Richard A. Couttenye [b,1], William S. Willis [a], Steven L. Suib [a,b,*], Paul T. Fanson [c], Hirohito Hirata [d], Masaya Ibe [d]

[a] *Department of Chemistry, University of Connecticut, Storrs, CT 06269-3060, USA*
[b] *Department of Chemical, Materials & Biomolecular Engineering, University of Connecticut, Storrs, CT 06269-3060, USA*
[c] *Toyota Motor Engineering and Manufacturing North America, Inc., Ann Arbor, MI 48105, USA*
[d] *Toyota Motor Company, Japan, 1 Toyota-cho, Toyota, Aichi 471-8572, Japan*

Received 26 July 2007; revised 25 October 2007; accepted 26 October 2007

Available online 26 November 2007

Abstract

Light hydrocarbons and H_2 can be used to enhance NO_x reduction efficiency and regenerate sulfur-poisoned NO_x storage catalysts, and therefore are valuable for automotive exhaust gas cleaning. The processing of hydrocarbons in an alternating current (AC) discharge nonthermal plasma reactor was studied for the instant generation of light hydrocarbons and H_2 at room temperature and atmospheric pressure. *n*-Octane and *n*-hexane were used as model hydrocarbons. Effects of hydrocarbon feedstock, electrode diameter, applied voltage, flow rate of carrier gas, gap size, and residence time of hydrocarbon molecules, were investigated systematically. Cracking is the only detected reaction during *n*-octane conversion (which might be very attractive for the cracking of heavy oil), and is the dominant reaction during *n*-hexane conversion. Catalytic dehydrogenation, catalytic addition, and noncatalytic cracking reactions, were discussed. The cleavage mode of single carbon–carbon bonds is revealed to be relevant to the carbon number of hydrocarbon molecules. Conversions, yields, power consumption, energy efficiencies, generation of hydrogen, etc, were determined and discussed. This study is of importance to novel processing of hydrocarbons at room temperature and atmospheric pressure, instant generation of hydrogen, cleaning of automotive exhaust gas, and chemistry in nonthermal plasma reactors.
© 2007 Elsevier Inc. All rights reserved.

Keywords: Hydrocarbon processing; Automotive exhaust gas; Nonthermal plasma; NO_x storage-reduction; Catalytic dehydrogenation; Hydrogen generation

1. Introduction

NO_x storage-reduction (NSR) catalysis technology was developed for the emission control of lean-burn gasoline and diesel engines, due to the difficulties for conventional three-way catalysts to remove NO_x from oxygen-rich exhaust gases [1,2]. The regenerating rich pulse is typically accomplished by engine control or by directly injecting diesel fuel into the exhaust stream. However, the long chain hydrocarbon molecules found in automotive fuel typically have very low reactivity. Much higher NO_x reduction efficiency could be achieved if the hydrocarbon fuel could first be converted on-board to lighter hydrocarbons such as ethylene (C_2H_4), propylene (C_3H_6), or H_2. In addition, these reducing agents, light hydrocarbons and H_2, are also more reactive for the regeneration of sulfur poisoned NO_x storage catalysts [1,3,4].

Conventional hydrocarbon cracking technologies [5] are not suitable for on-board automotive systems because of the need for catalyst warm-up time, a hydrogen source, or coke removal, etc. A possible alternative strategy is to use nonthermal plasma technology which has received considerable attention in the fields of chemistry and material processing [6]. In addition, catalysis technology has been successfully com-

* Corresponding author. Fax: +1 860 486 2981.
E-mail address: steven.suib@uconn.edu (S.L. Suib).
[1] Present address: Kraft Foods R&D Center, 801 Waukegan Road, Glenview, IL, 60025, USA.

0021-9517/$ – see front matter © 2007 Elsevier Inc. All rights reserved.
doi:10.1016/j.jcat.2007.10.024

bined with nonthermal plasma technology in various applications [7–13].

We reported the preliminary research on conversion of *n*-hexane over different electrode compositions in a PACT (plasma and catalysis integrated technologies) reactor, a type of nonthermal plasma reactor [7]. Herein we report studies on the processing of hydrocarbons in an alternating current (AC) discharge PACT nonthermal plasma reactor, where hydrogen or/and light alkanes/alkenes were produced instantly at room temperature and atmospheric pressure. *n*-Octane (n-C8) and *n*-hexane (n-C6) were used as model hydrocarbons. Effects of hydrocarbon feedstock, electrode diameter, applied voltage, flow rate of carrier gas, gap size, and residence time of hydrocarbon molecules, were studied systematically.

2. Experimental

2.1. PACT tubular reactor setup

The reactions were carried out in a tubular PACT reactor, as depicted in Fig. 1. The reactor consists of an exchangeable, cylindrical, nonporous inner metal electrode of 10 cm length and 8.0 (or 9.5) mm diameter, screwed onto a supporting metal rod, and a quartz tube (17.9 cm long, 9.85 mm i.d., and 12.55 mm o.d.) acting as dielectric separating outer and inner electrodes. Aluminum foil (10 cm long) is wrapped around this quartz tube and acts as the outer electrode. Nickel was electroplated onto copper rods at a thickness of 100 μm and these

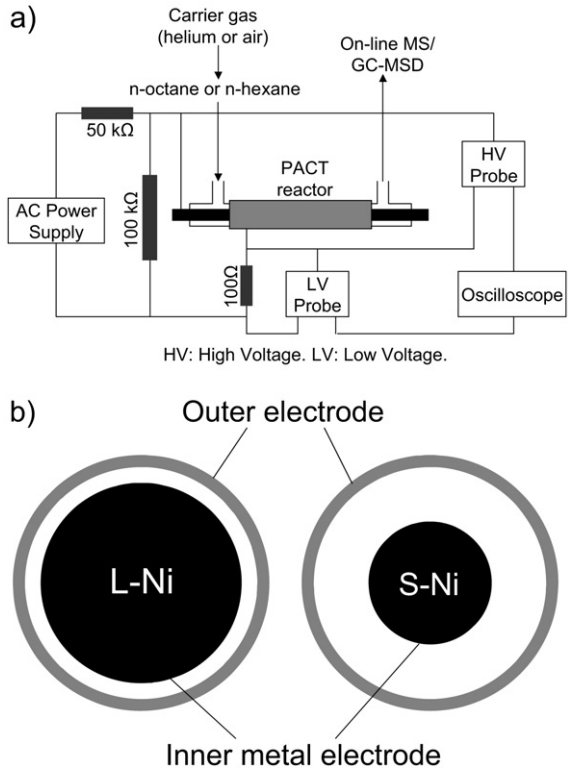

Fig. 1. Diagram of the PACT reactor system. (a) The circuit setup and PACT reactor setup. (b) Cross section of the PACT reactors. L-Ni: large-diameter nickel electrode. S-Ni: small-diameter nickel electrode.

Table 1
Plasma zone data for electrodes with different diameters

Inner electrode	Diam.[a] (cm)	Length[b] (cm)	SA[c] (cm^2)	Gap size[d] (mm)	Plasma zone vol.[e] (cm^3)
L-Ni[f]	0.950	10.000	29.845	0.175	0.532
S-Ni[g]	0.800	10.000	25.130	0.925	2.594

[a] Diameter of inner electrode.
[b] Length of inner electrode.
[c] Side surface area in plasma zone.
[d] The distance between the inner electrode and the tubular quartz barrier. The diameter of inner wall of quartz tube barrier is constantly 9.85 mm.
[e] The volume of the cavity between the inner electrode and the tubular quartz barrier, where a nonthermal plasma be generated by AC discharge and exists.
[f] Large-diameter nickel electrode.
[g] Small-diameter nickel electrode.

products were used as electrodes. The metal electrodes were obtained from Mitsubishi Materials Corporation. Table 1 shows detailed data on the types of the electrodes used in this research and the sizes of plasma zones.

2.2. Circuit setup

The circuit setup is also shown in Fig. 1. The high-voltage supply was 120 V AC (60 Hz). The high voltage was generated by an UHV-10 AC high-voltage power supply. A digital DL-1540 Yokogawa oscilloscope with a high-voltage probe (Tektronix P6025) and a low-voltage probe (Yokogawa 70996) was used to measure input voltage and input current of the PACT reactor. The voltage across a 100 Ω standard resistor in series with the reactor was used to determine the input current.

2.3. Experimental parameters and product analysis

In a typical experiment, a carrier gas (helium) was passed through a bubbler containing about 500 ml *n*-hexane liquid, at a flow rate of 44 ml/min, and the gaseous mixture was introduced into the PACT reactor at room temperature and atmospheric pressure. *n*-Hexane and *n*-octane feeds were purchased from J.T. BAKER and ALFA AESAR, respectively. *n*-Hexane feed contained 95% *n*-hexane and 5% hexanes including methyl cyclopentane and 3-methyl pentane. The reactor's inner metal electrode was connected to the high-voltage line, while the outer aluminum/quartz electrode was connected to the ground line.

During the experiments, the PACT reactor was not heated, and no significant temperature change was observed. For the purpose of simplification, the reactor was assumed to be an ideal plug flow reactor. The reaction system was vent to atmosphere, which maintained a constant reactor pressure at atmospheric pressure. The set carrier gas flow rate under these experimental conditions was 15, 44, 87, 145, or 218 ml/min. Due to the use of the dial of the UHV-10 HV supply and the consistency of tests, the set value of applied voltage under these experimental conditions was 5.4, 6.8, 8.2, 9.5, 10.6, or 12.0 kV. Unless specified otherwise, the reactor was run for 20 min to allow the system to come to equilibrium before a sample of the

Table 2
Feed supply rate, hydrocarbon (HC)-based space velocity (SV), and residence time of feed molecules at different flow rates of carrier gas helium[a]

Inner metal electrode	Type of HC feed	Carrier gas flow rate (ml/min)	Feed supply rate (g/h)	HC-based SV (h^{-1})	Res. time of feed mol (s)
L-Ni	*n*-Hexane	15	0.618	330	1.83
L-Ni	*n*-Hexane	44	3.370	1798	0.54
L-Ni	*n*-Hexane	87	4.773	2546	0.29
L-Ni	*n*-Hexane	145	6.190	3301	0.18
L-Ni	*n*-Hexane	218	9.446	5038	0.12
S-Ni	*n*-Hexane	15	0.618	68	8.91
S-Ni	*n*-Hexane	44	3.370	369	2.61
S-Ni	*n*-Hexane	87	4.773	522	1.42
S-Ni	*n*-Hexane	145	6.190	677	0.89
S-Ni	*n*-Hexane	218	9.446	1033	0.59
S-Ni	*n*-Octane	87	0.162	13	1.77

[a] Space velocity (SV) is defined here as volumetric flow rate of gaseous hexane through the reactor divided by the volume of the plasma zone of the reactor.

effluent was collected. Experimental parameters for *n*-octane or *n*-hexane conversion in the PACT reactor are listed in Table 2.

Product mixtures were analyzed by gas chromatography/mass spectroscopy (GC/MS) by a previously described method [7]. During each 20-min test, the amount of coke produced was negligible and was not counted in the calculation of yield data. Error bars represent standard deviations. The product mixture in the outlet of the PACT reactor was monitored continuously with a portable MKS-UTI MSS quadrupole residual gas analyzer mass spectrometer (MS).

2.4. Determination of power consumption and energy efficiency

The instantaneous power ($P_{i,t}$) delivered to a load (herein the PACT reactor) can be expressed as Eq. (1), where $V_{i,t}$ and $I_{i,t}$ are respectively the instantaneous voltage and instantaneous current:

$$P_{i,t} = V_{i,t} \times I_{i,t}. \quad (1)$$

Here $V_{i,t}$ is the instantaneous high voltage applied to the PACT reactor, which can be measured directly by the oscilloscope with high-voltage probes. The $I_{i,t}$ equals the current through the 100-Ω standard resistor. The voltage of the standard resistor can be measured directly by the oscilloscope with low-voltage probes. Therefore, the $I_{i,t}$ can be obtained using Ohm's law, so does the $P_{i,t}$. Fig. 2 shows an example of the $V_{i,t}$, $I_{i,t}$, and $P_{i,t}$ of the PACT reactor. The values of $P_{i,t}$ are used for the calculation of the average power (P_{avg}), the net average power that is consumed by the PACT reactor, which is used to determine the energy efficiency. Energy efficiency for converting a feed is defined here as the amount of the feed converted per Joule of electrical energy consumed. Energy efficiency for yielding products is defined here as the amount of products produced per Joule of electrical energy consumed.

3. Results and discussion

3.1. Conversion of n-octane and n-hexane in helium at different applied peak-to-peak (p-p) voltages

As shown in Table 2, hexane supply rate (i.e., the amount of hexane carried away by helium from the bubbler per hour), increased rapidly with increasing carrier gas flow rate. The octane supply rate listed in Table 2 is defined in a similar way, but is significantly less than the hexane supply rate (at the same helium flow rate) due to the low volatility of *n*-octane.

Residence time, also called space time, denotes the average time it takes for individual gaseous hydrocarbon molecules to pass through the plasma zone with a length of 10 cm, and equals the ratio of the plasma zone volume to the total volumetric flow rate of both carrier gas and hydrocarbon feed. The diameter of the inner metal electrode affects the volume of the plasma zone volume of the PACT reactor (Table 1), and consequently affects the residence time of feed molecules (Table 2).

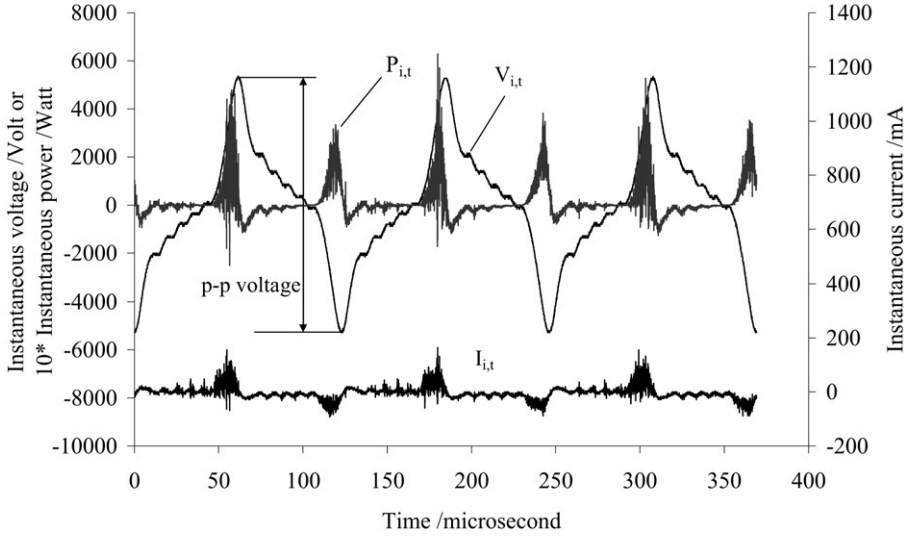

Fig. 2. Three periods of AC power, voltage, and current at applied peak-to-peak (p-p) voltage of 12.0 kV.

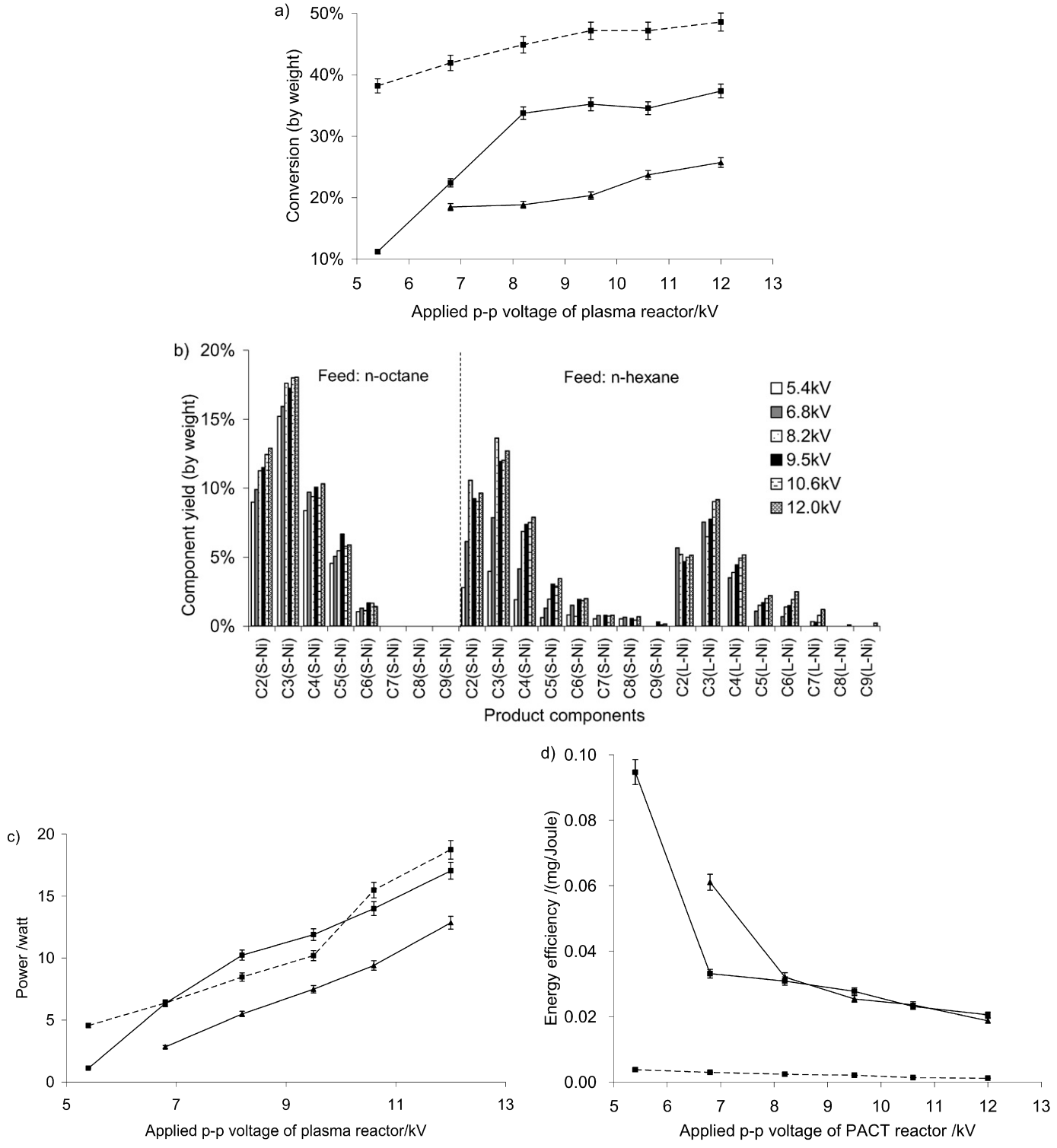

Fig. 3. Experimental results at different applied voltages. Flow rate of carrier gas helium: 44 ml/min for hexane tests and 87 ml/min for octane tests; (■) S-Ni electrode; (▲) L-Ni electrode; solid line: *n*-hexane feed; dashed line, *n*-octane feed. (a) Conversion vs applied voltage. (b) Yields of product components at different applied voltages. (c) Power vs applied voltage. (d) Energy efficiency vs applied voltage.

Fig. 3a shows that all of the octane and hexane conversions increased as the applied voltage was increased from low to high. Although the surface area of the large-diameter nickel electrode (L-Ni) is larger than that of the small-diameter nickel electrode (S-Ni), as shown in Table 1, the hexane conversions over L-Ni electrode were lower than those over S-Ni electrode. The residence time (2.61 s) of hexane molecules over S-Ni electrode is longer than that (0.54 s) over L-Ni electrode. Therefore, in a PACT reactor, the residence time of hydrocarbon molecules has significantly greater effects on hydrocarbon conversion than the

surface area of the inner metal electrode does. Longer residence time provides more chance for a molecule to be activated in the plasma zone, and therefore will produce higher conversion.

As shown in Fig. 3a, no reactions occurred at applied voltages below 5.4 kV. At 5.4 kV, the hexane/helium plasma was generated over S-Ni electrode, but cannot be generated over L-Ni electrode. And S-Ni electrode is actually less close to the outer electrode than L-Ni electrode, as shown in the gap size data in Table 1. These indicate that the residence time of feed molecules is the factor that affects the breakdown voltage (i.e., the minimum applied voltage to generate a plasma). Fig. 3a shows that, for S-Ni electrode, although the residence time of *n*-octane molecules (1.77 s) was shorter than that of *n*-hexane molecules (2.61 s), the *n*-octane conversions were higher than the *n*-hexane conversions. This indicates that, in the PACT reactor, cleavage of hydrocarbon molecules with a higher carbon number (e.g., *n*-octane C_8H_{18}) is likely easier than those with a lower carbon number (e.g., *n*-hexane C_6H_{14}). And this is consistent with the results of catalytic cracking of hydrocarbons in conventional tubular reactors [14]. A common reason for them is very likely because *n*-octane has lower activation energy (24.9 kcal/g mol) for cracking than *n*-hexane (36.6 kcal/g mol) [14].

The term C2 denotes the hydrocarbons, such as ethane and ethylene, that have two carbon atoms in each molecule. The terms C3, C4, and so on are defined similarly. For *n*-hexane conversion, the C6 products are mainly hexenes from the dehydrogenation of hexanes, with a small amount of hexane isomers from the isomerization of *n*-hexane. This suggests that hydrogen will be directly generated from the dehydrogenation of hexanes. The C7–C9 products are possibly part of the products of disproportionation reactions, such as the reaction between two C6 hydrocarbon (HC) molecules to form one C4HC molecule and one C8HC molecule. Although the mechanism of these disproportionation reactions remains unclear, the cracking of single carbon–carbon bonds and the recombination of produced fragments, such as radicals, hydride ions, carbocations, and/or carbanions, are likely involved in the formation of C7–C9 products. Free radical addition or/and electrophilic addition onto carbon–carbon double bonds are higher possible pathways for the formation of C7–C9 products in plasma conditions.

As shown in Fig. 3b, for *n*-hexane conversion over L-Ni electrode, C8 and C9 products were not produced until the applied voltage reached the highest value of 12.0 kV. This indicates that high applied voltages facilitate addition reaction more than low applied voltages do. This also indicates that nickel electrodes are not very catalytically active for addition reactions, and therefore could be good candidates for this research, because cracking reaction products (C2–C5) are favored while addition reaction products (C7–C9) are unfavorable. During *n*-hexane conversion, the differences between C2 and C4 yields for both S-Ni and L-Ni electrodes, did exist but were not significant. This indicates that the cracking of *n*-hexane is basically not dual-step cracking but single-step cracking. In the case of hexane conversion, the yields of C2–C5 products are significantly higher than those of C6–C9 products. These data suggest that cracking is the major reaction during *n*-hexane conversion, while other reactions such as dehydrogenation, isomerization, and addition are all minor reactions.

The product distribution for conventional catalytic cracking of *n*-hexane on HY zeolite is $C3 > C4 > C5 \gg C2$ [14]. This is different from the product distribution ($C3 > C4 \approx C2 > C5$) during *n*-hexane conversion in the PACT reactor, as shown in Fig. 3b. These data indicate that different mechanisms might involve in the conversion of hydrocarbon feed under different conditions.

Fig. 3b shows that only C2–C6 products were found during *n*-octane conversion. This suggests that cracking was likely the only reaction occurred during *n*-octane conversion. It seems like only simple cracking reactions, in the PACT reactor, could occur during the conversion of hydrocarbon molecules with a high carbon number (e.g., C_8H_{18}). And this might be very attractive for the cracking of heavy oil and is worth further research. The differences between C2 and C6 yields, and the differences between C3 and C5 yields in the case of *n*-octane conversion, are significant. This indicates that the cracking of *n*-octane was basically dual-step cracking. For example, *n*-octane (n-C8) was cracked to ethylene (C2) and hexane (C6), while the produced hexane was further cracked to C2/C4 hydrocarbons such as ethylene/butane or ethane/butene. Product output denotes the amount of a product or a group of products produced per hour, and is the function of yield and feed supply rate. Since the *n*-octane supply rate was much lower than the *n*-hexane supply rate, the outputs of the products during *n*-octane conversion are actually much lower than those during *n*-hexane conversion.

By and large, all of the yields shown in Fig. 3b showed an increasing trend as the applied voltage was increased from low to high. For *n*-hexane conversion, the yields of favorable C2–C5 products over S-Ni electrode were generally higher than those over L-Ni electrode at different applied voltages, while the yields of unfavorable C7–C9 products over L-Ni electrode were generally lower than those over S-Ni electrode.

The values of all average powers increased as the applied voltage was increased from low to high, as shown in Fig. 3c. Although there were significant differences on feed supply rates, the power consumptions during *n*-octane conversion over S-Ni electrode was very close to those during *n*-hexane conversion over S-Ni electrode. This indicates that the energy efficiency during *n*-octane conversion will be much lower than those during *n*-hexane conversion, as confirmed in Fig. 3d. As shown in Fig. 3c, the power consumption during *n*-hexane conversion over S-Ni electrode was higher than that during *n*-hexane conversion over L-Ni electrode. Although this is consistent with the fact that the hexane conversions over S-Ni electrode was higher than those over L-Ni electrode, the power consumption of a PACT reactor seems to be related with the gap size to some extent, of which the mechanism remains unclear.

Generally, the energy efficiencies shown in Fig. 3d all had maximum values at their lowest applied voltages, and all showed a decreasing trend as the applied voltage changed from low to high. The increase of applied voltage, therefore, will enhance the conversion but decrease the energy efficiency. Drastic drops in energy efficiencies at low power were observed during

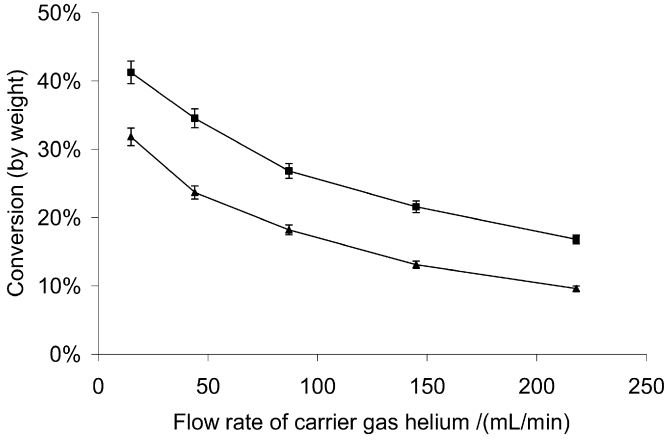

Fig. 4. Conversion vs flow rate of carrier gas helium during *n*-hexane conversion (applied voltage: 10.6 kV; (■) S-Ni electrode; (▲) L-Ni electrode).

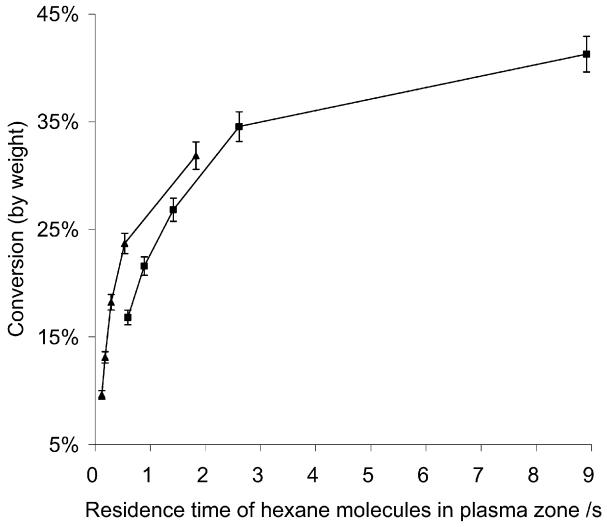

Fig. 5. Conversion vs residence time of hexane molecules during *n*-hexane conversion in helium (applied voltage: 10.6 kV; (■), S-Ni electrode; (▲) L-Ni electrode).

n-hexane conversion for both S-Ni and L-Ni electrodes. During *n*-hexane conversion, the energy efficiencies at breakdown voltages are significantly higher than those at higher voltages. In comparison with hexane conversion, the drop of the energy efficiency at low power during *n*-octane conversion was mild.

Assuming that the average bond dissociation energy of single carbon–carbon bonds is about 347 kJ/mol; thus, the theoretical maximum energy efficiency for cracking carbon–carbon bonds is about 2.882 E−03 mol/kJ (=1/(347 kJ/mol)). The highest energy efficiencies achieved during *n*-hexane conversion over S-Ni electrode, during *n*-hexane conversion over L-Ni electrode, and during *n*-octane conversion over S-Ni electrode, are 0.0946, 0.0610, and 0.0038 mg/J respectively, which equal 1.098 E−03, 0.708 E−03, and 0.033 E−03 mol/kJ respectively. The ratios of these practical energy efficiencies to the theoretical maximum energy efficiency are 38, 25, and 1%, respectively. These data show that, at these certain conditions, maximally 38, 25, and 1% of the energy consumed by the PACT reactor were respectively used for cracking single carbon–carbon bonds during *n*-hexane conversion over S-Ni electrode, during *n*-hexane conversion over L-Ni electrode, and during *n*-octane conversion over S-Ni electrode. To increase the *n*-octane supply rate, for example, via fuel injection, is possibly an important method to enhance the energy efficiency of *n*-octane conversion.

3.2. Conversion of n-hexane in helium at different carrier gas flow rates

As shown in Fig. 4, as the helium flow rate increased from 15 to 218 ml/min, the conversion rapidly decreased for both S-Ni and L-Ni electrodes. This is consistent with the decrease of residence time of feed molecules shown in Table 2. Furthermore, at each certain helium flow rate under a constant applied voltage of 10.6 kV, the conversion over S-Ni electrode was significantly higher than that over L-Ni electrode. Therefore, at the same applied voltage, the longer the residence time of feed molecules have, the higher the conversion can be obtained. This is possibly because that hydrocarbon molecules may have more opportunities to react when staying in the plasma zone for a longer time.

Fig. 5 shows that the conversions of *n*-hexane over L-Ni and S-Ni electrodes have increasing, and approximately parallel, trends as the residence time of hexane molecules increased. It shows that at the same residence time of hexane molecules, the conversion of hexane over L-Ni electrode was higher than that over S-Ni electrode. This is likely due to the effects of gap size and surface area of the electrode. As shown in Table 1, the gap size in the case of L-Ni electrode is smaller than that in the case of S-Ni electrode, while the surface area of L-Ni electrode is larger than that of S-Ni electrode. Compared with S-Ni electrode, an inner L-Ni electrode is closer to the outer electrode and therefore has a shorter distance for AC discharge, and provides larger surface area. Therefore, at the same residence time of hexane molecules, the conversion of hexane over L-Ni electrode could be higher than that over S-Ni electrode.

Fig. 5 also shows that, for both S-Ni and L-Ni electrodes, the conversions of *n*-hexane increased rapidly as the residence time of hexane molecules increased from 0.59 to 2.61 s (over S-Ni) or from 0.12 to 0.54 s (over L-Ni), and then the increasing trends slowed down significantly as the residence time of hexane molecules increased from 2.61 to 8.91 s (over S-Ni) or from 0.54 to 1.83 s (over L-Ni). These data indicate that overly high residence times of hexane molecules (such as 8.91 s for S-Ni and 1.83 s for L-Ni) are not favored, because the decreases of hexane supply rates were more significant than the increases of conversions, and could finally cause the feed conversion rate (defined as the amount of hydrocarbon feed converted per hour) to be very low.

Fig. 6a shows the effects of the electrode diameter and carrier gas flow rate on the product distribution observed in this reaction. For both S-Ni and L-Ni electrodes, the total yield of C2–C5 products was significantly higher than that of C6–C9 products, especially at low helium flow rates. This verifies again that cracking was the major reaction during *n*-hexane

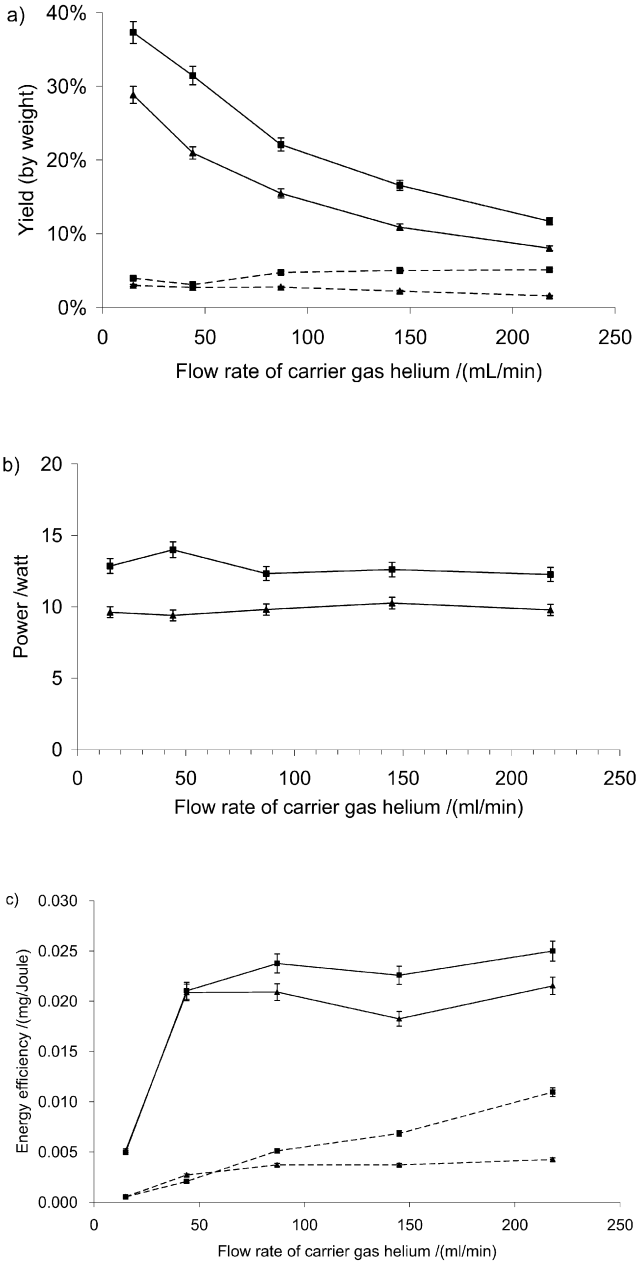

Fig. 6. Some experimental results during *n*-hexane conversion at different flow rates of carrier gas helium. Applied voltage: 10.6 kV; solid line: C2–C5 yield; dashed line: C6–C9 yield; (■) S-Ni electrode; (▲) L-Ni electrode. (a) Yield vs flow rate of carrier gas helium. (b) Power vs flow rate of carrier gas helium. (c) Energy efficiency vs flow rate of carrier gas helium.

conversion, whereas other reactions were all minor reactions. This also indicates that a longer residence time of hexane molecules will facilitate cracking reactions rather than other types of reactions. Both the total yield of C2–C5 products and the total yield of C6–C9 products over S-Ni electrode were greater than those over L-Ni electrode, basically because the conversion over S-Ni electrode was higher than that over electrode.

Fig. 6a also shows that for both S-Ni and L-Ni electrodes, the total yield of C2–C5 products decreased significantly as the helium flow rate was increased from 15 to 218 ml/min, whereas the total yield of C6–C9 products remained fairly constant as plotted versus the flow rate of carrier gas. This indicates that cracking reactions, which produces C2–C5 products, may have occurred primarily in the gas phase of the plasma zone rather that on the electrode surface, whereas the reactions to make C6 and larger molecules seemed unaffected by the flow rate of carrier gas and therefore may have occurred on the electrode surface rather than in the gas phase. Because the surface of the metal electrode is not involved, the cracking reactions in the gas phase are likely noncatalytic reactions and are dominated by the plasma, such as the residence time in plasma zone. The reactions on the electrode surface are basically catalytic reactions (e.g., the formation of hexenes via catalytic dehydrogenation and the formation of C7–C9 via catalytic addition), because the surface of the metal electrode (i.e., the catalyst) may involve in the absorption of feed molecules (or radicals/ions), formation of intermediates and products, and desorption of products. Once these interface processes reach an equilibrium, the catalytic reactions on electrode surface will become unaffected by the concentration of feed molecules in the gas phase, which is controlled by the flow rate of carrier gas [7].

Fig. 6b shows that for both S-Ni and L-Ni electrodes, the average power values underwent no considerable changes as the helium flow rate changed from 15 to 218 ml/min. This suggests that the carrier gas flow rate, which caused significant differences in hexane-based space velocity, has a very limited effect on average power consumption. The power consumptions during *n*-hexane conversion over S-Ni electrode were a little higher than those over L-Ni electrode. Although this is consistent with the fact that the hexane conversions over S-Ni electrode are higher than those over L-Ni electrode, the effect of the gap size on the power consumption of a PACT reactor cannot be ruled out and seems to play an important role, of which the mechanism remains unclear. Figs. 3c and 6b suggest that the power consumption of a PACT reactor is dominated by applied voltage, but not significantly affected by carrier gas flow rate and HC-based space velocity.

Fig. 6c shows that for both S-Ni and L-Ni electrodes during *n*-hexane conversion, the energy efficiencies for yields of favorable C2–C5 cracking products and for yields of C6–C9 products all have their minimum values at the lowest helium flow rates of 15 ml/min, and all showed increasing trends as the helium flow rate changed from 15 to 218 ml/min. This indicates that overly long residence time of feed molecules at the lowest helium flow rate, will waste considerable electrical energy and greatly decrease the energy efficiency.

The data of Figs. 4–6 suggest that within the set values, 44 ml/min is the optimal flow rate of carrier gas helium for both S-Ni and L-Ni electrodes in the PACT reactor, at which high conversion, high yield of favorable C2–C5 products, low yield of C6–C9 products, and satisfactory energy efficiencies can be achieved. Figs. 3d and 6c show that applied voltage, flow rate of carrier gas, diameter of inner metal electrode, and type of hydrocarbon feedstock, all affect the energy efficiency of a PACT reactor.

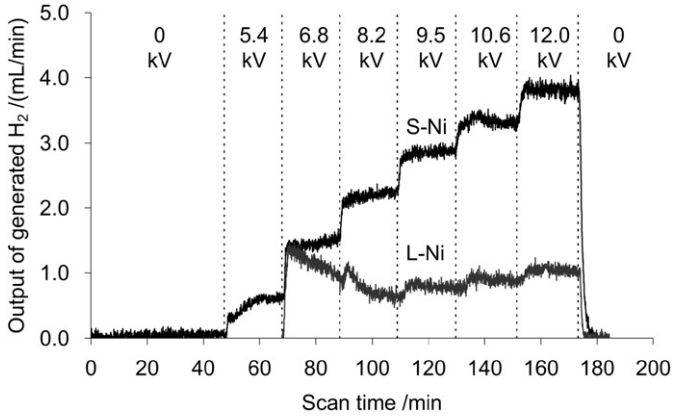

Fig. 7. Quantitative online detection of generated hydrogen by mass spectrometry during *n*-hexane conversion (flow rate of carrier gas helium: 44 ml/min).

3.3. Detection of hydrogen and methane during n-hexane conversion in helium by online mass spectrometer

The outputs of generated hydrogen during *n*-hexane conversion over L-Ni and S-Ni electrodes were determined via online mass spectrometry detection and calibrated using standard gas mixtures. As shown in Fig. 7, before a plasma was generated, no reactions occurred in the PACT reactor. Once a plasma was generated at an applied voltage of 6.8 kV over L-Ni electrode or 5.4 kV over S-Ni electrode, reactions occurred and hydrogen was produced immediately. Once the applied voltage was turned off, as shown from the highest applied voltage of 12.0 to 0 kV, reactions stopped immediately and the partial pressure of hydrogen dropped drastically, and then disappeared quickly. These data verify that *n*-hexane conversion reactions can occur instantly, and hydrogen can be generated instantly under a suitable applied voltage. These data also explain the relationship between the plasma reactor and an electrode catalyst. The catalyst itself (i.e., the metal electrode) cannot catalyze any hydrocarbon reactions at room temperature due to the existence of an energy barrier, which must be overcome for activation of the molecules. In comparison with conventional tubular reactors, the function of a PACT reactor is to provide electrical energy rather than thermal energy to activate the molecules at room temperature, and also to sustain the plasma status through continuously supplying AC discharge to the plasma zone. Once plasma is generated, feed molecules will be ionized and may be converted into products spontaneously (i.e., noncatalytically) or catalytically. Catalysts like the inner metal electrode of a PACT reactor then can function in the plasma zone to introduce ionized and dissociated species into special reaction pathways and produce products with special selectivities.

Fig. 7 also shows that the output of hydrogen over S-Ni electrode increased stepwise as the applied voltage was increased stepwise from 5.4 to 12.0 kV, and was significantly higher than that over L-Ni electrode. The trend of hydrogen production over L-Ni shows that dehydrogenation at higher applied voltage (i.e., 9.5–12.0 kV) seems more stable than that at lower applied voltage (i.e., 6.8–8.2 kV). The maximum output of generated hydrogen during *n*-hexane conversion over L-Ni electrode was 1.15 ml/min, which was significantly less than the maximum output of 3.90 ml/min over S-Ni electrode. Analysis of product components by GC/MSD shows that catalytic dehydrogenation of hexane is the source of hydrogen and hexenes. These data verify the fact that catalytic dehydrogenation was facilitated by the employment of S-Ni electrode more than the employment of L-Ni electrode. This is likely due to the longer residence time of hexane molecules over S-Ni electrode than that over electrode. Longer residence time means longer reaction time, which provides more opportunities for the catalytic dehydrogenation of hexanes to occur. Methane is not favored for this study due to its high chemical stability and consequent poor consumption during steam reforming. As detected with mass spectrometry (MS), methane was produced during *n*-hexane conversion in the PACT reactor but its concentration was very low (less than 1%) [7]. No methane peak was observed through GC/MS analysis, although the 150-m length PETROCOL™ DH150 capillary column installed in the GC/MS is capable of detecting light hydrocarbons including methane. Mass spectroscopy (MS) studies of hydrocarbons were done in our previous report [7] and are not shown in this paper.

4. Conclusion

The processing of *n*-octane and *n*-hexane in an alternating current (AC) discharge PACT (plasma and catalysis integrated technologies) reactor, which instantly produce hydrogen or/and light alkanes/alkenes at room temperature and atmospheric pressure, were systematically studied. In the PACT reactor, cleavage of hydrocarbon molecules with high carbon number (e.g., *n*-octane C_8H_{18}) is likely to be easier than those with low carbon number (e.g., *n*-hexane C_6H_{14}). Cracking is the only detected reaction during *n*-octane conversion (which might be very attractive for the cracking of heavy oil), and is the dominant reaction during *n*-hexane conversion. Cleavage mode of single carbon–carbon bonds in the PACT reactor is relevant to the carbon number of hydrocarbon molecules: the cracking of *n*-hexane is basically a single-step process while that of *n*-octane is basically a dual-step process. Cracking reactions are likely noncatalytic reactions in the gas phase, while the formation of C6 (i.e., hexenes)/H_2 via catalytic dehydrogenation and the formation of C7–C9 via catalytic addition are likely catalytic reactions on the electrode surface. The diameter of inner metal electrode affects the residence time of feed molecules as well as the gap size, and will consequently affect conversion, yield, power consumption, energy efficiency, and breakdown voltage of a plasma. Applied voltage and residence time of feed molecules have significant effects on the conversions of hydrocarbons. At the same residence time of hexane molecules, the conversion of *n*-hexane over the large-diameter nickel electrode could be greater than that over the small-diameter nickel electrode. Power consumption of a PACT reactor is dominated by applied voltage, but is not significantly affected by carrier gas flow rate and HC-based space velocity. Applied voltage, flow rate of carrier gas, diameter of inner metal electrode, and the type of HC feed, all affect the energy efficiency of a PACT reactor. The output of hydrogen is significantly affected by applied voltage and electrode diameter.

Acknowledgments

We thank Dr. Francis Galasso for helpful suggestions, Toyota Motor Corporation and The Chemical, Geosciences, and Biosciences Division, Office of Basic Energy Sciences, Office of Science, US Department of Energy (DOE) for financial support of this research.

References

[1] W.S. Epling, L.E. Campbell, A. Yezerets, N.W. Currier, J.E. Parks II, Catal. Rev. Sci. Eng. 46 (2004) 163–245.
[2] T. Kanazawa, Catal. Today 96 (2004) 171–177.
[3] M. Takeuchi, S. Matsumoto, Top. Catal. 28 (2004) 151–156.
[4] S. Matsumoto, Y. Ikeda, H. Suzuki, M. Ogai, N. Miyoshi, Appl. Catal. B 25 (2000) 115–124.
[5] G. Ertl, H. Knozinger, J. Weitkamp (Editors-in-Chief) Handbook of Heterogeneous Catalysis, VCH, Weinheim, 1997, p. 1955, 2017.
[6] A. Grill, Cold Plasma in Materials Fabrication (from Fundamentals to Applications), IEEE Press, New York, 1994, p. 58, 109.
[7] Y. Xing, Z. Liu, R.A. Couttenye, W.S. Willis, S.L. Suib, P.T. Fanson, H. Hirata, M. Ibe, J. Catal. 250 (2007) 67–74.
[8] Y.S. Mok, Y.J. Huh, Plasma Chem. Plasma Process. 25 (2005) 625–639.
[9] X. Chen, S.L. Suib, Y. Hayashi, H. Matsumoto, J. Catal. 201 (2001) 198–205.
[10] S.L. Brock, M. Marquez, S.L. Suib, Y. Hayashi, H. Matsumoto, J. Catal. 180 (1998) 225–233.
[11] X. Chen, J. Rozak, J.-C. Lin, S.L. Suib, Y. Hayashi, H. Matsumoto, Appl. Catal. A 219 (2001) 25–31.
[12] F. Spiess, S.L. Suib, K. Irie, Y. Hayashi, H. Matsumoto, Catal. Today 89 (2004) 35–45.
[13] J. Luo, S.L. Suib, Y. Hayashi, H. Matsumoto, J. Phys. Chem. A 1999 (2004) 6151–6161.
[14] B.W. Wojciechowski, A. Corma, Catalytic Cracking: Catalysts, Chemistry, and Kinetics, Dekker, New York, 1986, p. 130, 136.